

Measuring the Unique Identifiers of Topological Order Based on Boundary-Bulk Duality and Anyon Condensation

Yong-Ju Hai^{1#}, Ze Zhang^{1#}, Hao Zheng^{1,2}, Liang Kong^{*1,2}, Jiansheng Wu^{*1,2}, Dapeng Yu^{1,2}

¹*Department of Physics and Institute for Quantum Science and Engineering,*

²*Guangdong Provincial Key Laboratory of Quantum Science and Engineering,*

Southern University of Science and Technology, Shenzhen 518055, P. R. China.

[#]*These authors contributed equally to this work*

Abstract

A topological order is a new quantum phase that is beyond Landau's symmetry-breaking paradigm. Its defining features include robust degenerate ground states, long-range entanglement and anyons. It was known that R - and F -matrices, which characterize the fusion-braiding properties of anyons, can be used to uniquely identify topological order. In this article, we explore an essential question: how can the R - and F -matrices be experimentally measured? By using quantum simulations based on a toric code model with boundaries and state-of-the-art technology, we show that the braidings, i.e. the R -matrices, can be completely determined by the half braidings of boundary excitations due to the boundary-bulk duality and the anyon condensation. The F -matrices can also be measured in a scattering quantum circuit involving the fusion of three anyons in two different orders. Thus we provide an experimental protocol for measuring the unique identifiers of topological order.

Topological orders are defined for gapped many-body systems at zero temperature. They were first discovered in 2-dimensional (2d) fractional quantum Hall systems, and are new types of quantum phases beyond Landau's symmetry-breaking paradigm¹⁻¹⁷. They also provide the physical foundation of fault-tolerant quantum computers¹⁸⁻²².

The mathematical characterization of a 2d topological order was known⁵. In reality, only the modular data, as an ingredient of the characterization, is known to be physically measurable^{6,7,23-28}. This motivated a folklore belief among experts that the modular data might be complete²⁹. A recent mathematical result³⁰, however, suggests that it is incomplete. A 2d topological order permits particle-like topological excitations, called anyons. When two anyons are braided (exchanged), a "phase factor", called an R -matrix, is presented in their wavefunctions (as illustrated in Fig.1a). Furthermore, two anyons can be fused together to produce a new anyon, from one or several possible outcomes. If we fuse three anyons a , b and c in two different ways, $((ab)c)$ and $(a(bc))$, where parentheses indicates the order of the fusion, the first set of fused states spans the same Hilbert space as the second one. The F -matrix is the transformation matrix between these two bases (as illustrated in Fig.1b). Mathematically, it was proved that the R -matrices and F -matrices uniquely determine the topological order^{4,5}. Consequently, they can serve as the unique identifiers of a topological order.

Therefore, the essential question is whether R -matrices (braidings) and F -matrices are physically measurable? The difficulty of measuring the R -matrices are twofold. The first one is that different (gauge choices of) R -matrices might define the same topological order. The second one

is that by the definition of braiding if we move one anyon along a semicircle around another anyon of a different kind in the bulk, the final state is so different from the initial one that there's no well-defined phase factor. The key to overcoming these two difficulties is to use the boundary-bulk duality and the anyon condensation on the boundaries^{31–35}. The main idea is that the braidings among bulk anyons are determined by the half braidings among boundary excitations, and these half braidings can be measured by moving one boundary excitation around another one along a semicircle near the boundary. We find different (but gauge equivalent) R -matrices are associated to different boundaries of the same 2d topological order. When the boundary is gapped, certain bulk anyons are condensed on the boundary, thus can be created or annihilated on the boundary by local operators. By creating an anyon at the boundary then half braiding it with another anyon then annihilating it on the boundary, we obtain a final state which differs from the initial state only by a phase factor (R -matrix), thus overcome the second difficulty. We also show that the F -matrices are measurable using a quantum circuit involving the fusion of three anyons in different orders. As a consequence, we provide a protocol for experimentally measuring the R -matrices and F -matrices.

We demonstrate this idea by means of quantum simulation using a toric code model with gapped boundaries. As the simplest example of Z_2 topological order, the toric code model is a useful platform for demonstrating anyonic statistics¹⁸. It is defined on a 2d square lattice consisting of two kinds of plaquettes with qubits on their edges, as illustrated in Fig.1c.

The Hamiltonian is a sum of all four qubit interaction terms for the plaquettes (stabilizer

operators) in the lattice:

$$H = - \sum_{\text{white plaquettes}} A_p - \sum_{\text{blue plaquettes}} B_p \quad (1)$$

The operators $A_p = \prod_{j \in \partial p} \sigma_j^x$ and $B_p = \prod_{j \in \partial p} \sigma_j^z$ are the plaquette operators acting on the four qubits surrounding white plaquettes and blue plaquettes respectively, as shown in Fig.1c α_1 and α_2 . Here σ_j^x and σ_j^z are the x -component and z -component of Pauli matrices, respectively, acting on the j -th of the four qubits for each plaquette. All of the above plaquette operators commute with each other, and their eigenvalues are ± 1 . The ground state (or vacuum, denoted by 1) of the system is the state in which all of the plaquette operators are in $+1$ eigenstates. Anyons can be created in pairs via string operators. As shown in Fig.1c α_3 and α_4 , the blue (red) string operator, consisting a sequence of σ_j^x (σ_j^z) operators acting on all qubits in the string, creates a pair of m anyons (e anyons) on the blue (white) plaquettes at the two ends of the string. The fusion of anyons can produce new types of anyons. The fusion rules are expressed as follows: $e \otimes e = m \otimes m = 1$, $e \otimes m = \varepsilon$.

Anyons can be braided. As illustrated in Fig.1c α_5 , when an m anyon is moved around an e anyon along a full circle (double braiding), it produces an overall phase of -1 between the final and the initial states. This phase relationship can be encoded by the S -matrices as illustrated in Fig.1c α_5 . Another important type of data is the topological spins of the anyons, encoded in T -matrices. The S -, T -matrices were believed by many to characterize a topological order uniquely, and, in the case of toric code, can be measured by experiments^{18,23,26}. It was shown recently that S -, T -matrices are, however, inadequate to uniquely identify topological order³⁰. For such unique identification, we need the R -matrices (braidings) and F -matrices. The R -matrices are actually

phase factors for the anyons in toric code model since the anyons here are Abelian. Two typical R -matrices for the toric code are $R_{me}^\varepsilon = -1$ and $R_{em}^\varepsilon = +1$. The measurement of the R -matrices are the main focus of this article.

The key to measuring the braidings (R -matrices) is to make use of the boundaries due to the boundary-bulk duality^{31,32} and the anyon condensation on the boundaries³³. There are two topologically distinct boundary types in the toric code²², namely the white boundaries (known as the smooth boundaries in the original vertex-plaquette form of toric code model) and the blue boundaries (rough boundaries in the original form), as shown in Fig.1c. When an m anyon approaches a white boundary, it disappears completely, or equivalently, condenses to the vacuum state. An e anyon cannot pass and becomes a boundary excitation. Therefore, the boundary excitations on a white boundary are $\{1, e\}$, and the bulk anyons are mapping to the boundary excitations as $1, m \mapsto 1, e, \varepsilon \mapsto e$ (as illustrated in Fig.2a). At a blue boundary, e anyons disappear and m anyons remain. Therefore, the blue boundary excitations are $\{1, m\}$ and the corresponding bulk-to-boundary map is $1, e \mapsto 1, m, \varepsilon \mapsto m$.

It turns out that bulk anyons can be uniquely determined by the excitations at either of these boundaries³¹⁻³³. For example, let us consider a white boundary, where m anyons condense. On this boundary, m and 1 belong to the same topological sector, i.e. $m = 1$. However, when an m is moved into the bulk, it is automatically endowed with additional structures called the *half braidings*. These half braidings can be measured by moving the m around a 1 or e along a semicircle near the boundary, as illustrated by Fig.1c α_7 . It is easy to check that moving an m

around a 1 along a semicircle does not result in a phase difference, whereas moving an m around an e along a semicircle results in a phase difference of -1 . Consequence, an m anyon in the bulk can be characterized by the following triple:

$$m = (1, 1 \otimes 1 = 1 \xrightarrow{1} 1 = 1 \otimes 1, 1 \otimes e = e \xrightarrow{-1} e = 1 \otimes e), \quad (2)$$

where the first component means that the $m = 1$ on the boundary and the second and the third components are the half braidings, which are physically measurable quantities. Therefore, bulk anyons are actually boundary excitations equipped with half braidings. In this way, we can recover all four bulk anyons in the forms of four triples (as illustrated in Table.1a and Fig.2b).

Furthermore, the braidings among these four anyons can be defined by the half braidings³⁶.

For example, we can obtain the following braiding,

$$m \otimes e = 1 \otimes e \xrightarrow{-1} e \otimes 1 = e \otimes m. \quad (3)$$

Here we have used $m = 1$ on the boundary and the half braiding -1 on the boundary (as illustrated in Fig.2c). Thus, we obtain $R_{me}^\varepsilon = -1$. In addition, since m condenses ($m = 1$) on the boundary, $R_{em}^\varepsilon = 1$ (For R_{bm}^c , b is the moving anyon and m is the anyon fixed on the boundary. Since $m = 1$ on the boundary, $R_{bm}^c = 1$ for an arbitrary b anyon. For R_{mb}^c , b is the fixed anyon on the boundary, and m is the moving anyon. Half braiding is applied in this case). All of the braidings of bulk anyons can be obtained in this way, as illustrated in Tabel.1b and Fig.2c. Thus, we can obtain the bulk braidings from the boundary half braidings, which are measurable. Note that this correspondence can be built by considering a virtual boundary in the bulk, and thus a one-to-one mapping from the bulk braidings to the boundary half braidings can be obtained (as illustrated in Fig.2c).

There are two equivalent sets of bulk braidings, either of which can completely characterize the bulk anyons (as illustrated in Fig.2c). Similarly, we can easily express all braidings among the bulk anyons in terms of half braidings as illustrated in Table.1b and Fig.2d. Double braidings can be obtained from the bulk braidings by combining the braidings as shown in Fig.2c.

In our experiments, we use nuclear magnetic resonance (NMR) qubits to demonstrate the half braiding operations on a the blue (smooth) boundary and the measurement of the F -matrices.

We mainly focus on the measurement of $R_{me}^\varepsilon = -1$ since it is the most important nontrivial phase factor in the toric code. For the 3-qubit case (Fig.3a), the Hamiltonian and the ground state $|\varphi_g\rangle$ of the triangular cell are shown in Fig.3e. The excited state $|\varphi_e\rangle$ can be obtained via a σ_z rotation of qubit 1 in the ground state leading to two e anyons on the lower two vertices. In this system, two different braiding processes can be performed by moving m along either Path 1 or Path 2. Braiding along Path 1 results in overall phase factors of $+1$ for the ground state and -1 for the excited state since in the latter case, a half braiding of m around e is performed. In contrast, Path 2 is a trivial path, meaning that braiding along it does not generate any phase factor difference. To measure the phase factor difference, we prepare an initial state that is a superposition of the ground state and excited state, $|\varphi_g\rangle + |\varphi_e\rangle$. Then, half braidings along Path 1 and Path 2 give rise to final states of $|\varphi_g\rangle - |\varphi_e\rangle$ and $|\varphi_g\rangle + |\varphi_e\rangle$, respectively, which can be identified by quantum state tomography. The 4-qubit case is similar, as shown in Fig.3b and Fig.3e. The corresponding quantum circuits for this experiment are shown in Fig.3c.

In Fig.4, we present the state tomography results obtained after running these quantum cir-

cuits on our NMR qubit platform. We can see that after moving m along Path 2, we obtain a final state that is the same as the initial state. In contrast, after moving m along Path 1, we obtain a final state that is completely different from the initial state, which is due to the phase factor of -1 induced by the half braiding of m around e . Thus we obtain the braiding in forms of the R -matrices, $R_{me}^\varepsilon = -1$. In principle, all other braidings can be similarly obtained.

In general, a half braiding (denoted as \hat{H}_f) leads to a phase factor for Abelian anyons, which can be measured by means of a ‘scattering’ circuit with one additional ancilla control qubit²⁶, as shown in Fig.3d. The state before half braiding is prepared as the initial state $|\varphi_i\rangle$, and the half braiding is performed as a controlled operation. The global phase generated by half braiding is obtained from the two expectation values $\langle\sigma_z\rangle$ and $\langle\sigma_y\rangle$ on the ancilla qubit through the relations $\langle\sigma_z\rangle = \text{Re}(\langle\varphi_i|\hat{H}_f|\varphi_i\rangle)$ and $\langle\sigma_y\rangle = \text{Im}(\langle\varphi_i|\hat{H}_f|\varphi_i\rangle)$. This method can also be applied to the non-Abelian anyon case, in which the measured values are the matrix elements of the R -matrix. This circuit is tested for m - e half braiding on a 3-qubit plaquette on NMR qubits as a proof-of-principle. $R_{me}^\varepsilon = -1$ theoretically corresponds to an exchange statistics phase of π , and we obtain values of $(1.027 \pm 0.001)\pi$ in the experiment.

The F -matrices can be measured by means of a similar ‘scattering’ circuit²⁶, as shown in Fig.5c. In this article, we show the measurement of a typical matrix F_{eem}^m . The initial state before fusion is prepared as the ground state $|\varphi_i\rangle$ without any anyons. Two controlled operations $\hat{A}_{1,2}$ are applied representing two fusion processes using different fusion orders to fuse two e anyons and an m , into an m anyons (illustrated in Fig.5a). The global phase generated by the different

fusion orders, F_{eem}^m , is obtained from the two expectation values $\langle\sigma_z\rangle$ and $\langle\sigma_y\rangle$ of the ancilla qubit. We experimentally measure $\langle\sigma_4^z\rangle$ and $\langle\sigma_4^y\rangle$ and obtain typical values of $\langle\sigma_4^z\rangle = 0.712 \pm 0.006$ and $\langle\sigma_4^y\rangle = 0.177 \pm 0.004$. We normalize them such that their square sum to 1 and obtain the angle $\theta = \arctan(\langle\sigma_4^y\rangle/\langle\sigma_4^z\rangle) = (0.077 \pm 0.002)\pi$, which is close to the theoretical value 0. Thus, we verify that $F_{eem}^m = 1$ in this experiment.

In summary, we experimentally measure anyon braidings (R -matrices) through the boundary-bulk duality, that is, bulk anyons are those boundary excitations equipped with half braidings, and bulk anyon braidings can be obtained from boundary excitation half braidings. Two difficulties that arise in the measurement of R -matrices, as noted in the introduction, can be overcome by means of the boundary-bulk duality and the anyon condensation on the boundaries: 1) if we instead consider the blue boundary, where e anyons condense, we will obtain another set of the R -matrices that is gauge equivalent to what is measured here, and 2) if an anyon is created on the boundary, half braided with another anyon, and then annihilated on the boundary, the final state and initial state differ only by a phase factor. These two difficulties seem to be technical problems, but they are actually related to the following essential question: what are the fundamental quantities that characterize topological order? This question is similar to the following one: which is the fundamental quantity for an electromagnetic field, the magnetic field/electric field or the vector potential/scalar potential? It would seem that since the vector potential is a gauge-dependent quantity, which means that it is not unique, it should not be measurable. However, the Aharonov-Bohm effect shows that when a particle passes through a region where the magnetic field is zero but the vector potential is nonzero, the phase of the wavefunction is shifted³⁷. This proves that the

vector potential, rather than the magnetic field, is the fundamental physical quantity. The relation between the double braiding and braiding of anyons is similar to that between the magnetic field and the vector potential. For a double braiding of two anyons, the spatial configuration of the final state is the same as that of the initial state, so the effect of the anyonic statistics can be measured by comparing the phase (it is a unitary matrix for non-Abelian anyons) before and after the double braiding. But for a braiding, i.e. an exchange in positions of two anyons, the spatial configuration of the final state is different from that of the initial state if these two anyons are of different kinds, which makes it unmeasurable in bulk. Furthermore, the R -matrices (braidings) are not unique for a given topological order. Therefore, it would seem that double braidings should be the fundamental quantities for topological orders. However, our experiments have demonstrated the important fact that braidings, rather than double braidings, are the fundamental physical quantities for topological orders. The F -matrices can also be measured using a ‘scattering’ quantum circuit involving the fusion of three anyons in different orders. The S -, T -matrices can be calculated from the R -, F -matrices^{4,5}. Thus, we provide an experimental protocol for uniquely identifying topological orders. Although our results are obtained on only a few qubits, the conclusion are applicable to large systems since the toric code is at a fixed point and the conclusion is independent of the system size³⁸. Furthermore, our boundary-bulk duality between bulk anyons and boundary excitations and the correspondence between bulk anyon braidings and boundary excitation half braidings also holds for other topological orders, even for non-Abelian anyons such as Fibonacci anyons and semions³². The idea of measuring the half braidings should also be useful to the experimental study of gapless boundaries^{34,35}. For a 2d topological order with chiral gapless boundaries, one can apply the

folding trick to embed the measurability problem to that of a double-layered system with only gapped boundaries. Given the special role of anyon braidings and topological orders in topological quantum computation and strongly correlated systems, our work has potential applications not only in uniquely identifying these exotic phases of matter but also in describing the interplay of bulk physics and boundary physics in topological systems. The recently proposed surface codes, using toric code with boundary and geometric defects, provide a scheme for practical large-scale quantum computation³⁹. The existence of boundaries and defects provides myriad possibilities for the manipulation of topological quantum states^{40,41}. It will be interesting to consider a topological quantum computation system in which bulk anyon braidings, boundary excitation half braidings and anyon condensation play significant roles; such an investigation is left for future work.

Methods

Our experiments are accomplished by means of our NMR quantum computer. Our 3, 4-qubit system is a sample of ^{13}C -labeled trans-crotonic acid molecules dissolved in d_6 -acetone. The sample consists of four ^{13}C atoms, as shown in Fig.5a, and all experiments are conducted on a Bruker Ascend NMR 600 MHz spectrometer at room temperature.

In the first experiment, our goal is to show an experimental proof-of-principle demonstration of the half braidings on a gapped boundary and show the effect of the nontrivial phase factor induced by it. That is, we create a condensed m anyon at the boundary and move it around a boundary excitation e along a semicircle; this is the most important nontrivial half braiding in the toric code. The experimental setup and quantum circuits are illustrated in Fig.3a-c, and the

specific quantum states involved can be seen in Table 1. The experiment can be divided into three steps: 1) preparing the initial state, i.e., a superposition of the ground state and the excited state; 2) performing half braiding by means of a series of single-qubit rotation operators; and 3) measuring the final state and using quantum state tomography to obtain the density matrix of the final state.

For Path 1, we obtain a final state that is different from the initial state due to the nontrivial phase factor induced by m - e half braiding. For Path 2, we obtain a final state that is the same as the initial one. We also calculate the average fidelity between the theoretical and experimental results of the half braiding operation. The average fidelities for Path 1 and Path 2 are 96.37% and 96.67% for the 3-qubit system, and are 95.23% and 95.21% for the 4-qubit system.

In the second experiment, to directly measure the phase factor induced by half braiding, the state before half braiding is prepared as the initial state $|\varphi_i\rangle$ with fidelity 95.32%, and the half braiding is performed as a controlled operation, as shown in Fig.4d. Finally, the two expectation values $\langle\sigma_z\rangle$ and $\langle\sigma_y\rangle$ on the ancilla qubit are measured to obtain the real and imaginary parts of the phase factor generated by half braiding from $\langle\sigma_z\rangle = \text{Re}(\langle\varphi_i|\hat{H}_f|\varphi_i\rangle)$ and $\langle\sigma_y\rangle = \text{Im}(\langle\varphi_i|\hat{H}_f|\varphi_i\rangle)$. The measurement of m - e half braiding on 3-qubit plaquette is performed using this circuit.

In the third experiment, to measure F -matrice F_{eem}^m , we choose $Q3$ in the molecule (Fig.4a) as the control qubit to reduce the complexity of the circuit since only C-not gates between the neighboring qubits are available. $Q1$, $Q2$ and $Q4$ in the molecule represent $Q1$, $Q2$ and $Q3$ in the circuit (Fig.4a), respectively. The ground state $|\psi_g\rangle$ of the 3-qubit toric code model is prepared with a fidelity of 92.96%. Then, the operators $\hat{A}_1^\dagger = (\sigma_3^x \sigma_3^z)^\dagger$ and $\hat{A}_2 = \sigma_2^z \sigma_3^x \sigma_1^z$ (corresponding

to Path 1 and Path 2 in Fig.5a), which represent two different orders of fusion of three anyons, are applied to the 3-qubit toric code under the control of qubit $Q4$. We measure $\langle \sigma_4^z \rangle$ and $\langle \sigma_4^y \rangle$ of the control qubit to obtain the overlap of the two final states from two paths, thus obtain the angle $\theta = \arctan(\langle \sigma_4^y \rangle / \langle \sigma_4^z \rangle)$ and $F_{em}^m = \exp(i\theta)$.

Detailed theory and detailed descriptions of the experimental processes and data are provided in the Supplementary Material.

1. Wen, X.-G., Topological orders in rigid states. *Int. J. Mod. Phys. B.* **4**, 239-271 (1990).
2. Wen, X.-G. & Niu, Q., Ground state degeneracy of the FQH states in presence of random potential and on high genus Riemann surfaces. *Phys. Rev. B.* **41**, 9377-9396 (1990).
3. Wen, X.-G., Topological orders and Chern-Simons theory in strongly correlated quantum liquid. *Int. J. Mod. Phys. B.* **5**, 1641-1648 (1991).
4. Moore, G. & Seiberg, N., Classical and quantum conformal field theory. *Commun. Math. Phys.* **123**, 177-254 (1989).
5. Kitaev, A.Y., Anyons in an exactly solved model and beyond. *Ann. Phys.* **321**, 2-111 (2006).
6. Kitaev, A. & Preskill, J., Topological entanglement entropy. *Phys. Rev. Lett.* **96**, 110404 (2006).
7. Levin, M. & Wen, X.-G., Detecting topological order in a ground state wave function. *Phys. Rev. Lett.* **96**, 110405 (2006).

8. Tsui, D. C., Stormer, H. L. & Gossard, A. C., Two-dimensional magnetotransport in the extreme quantum limit. *Phys. Rev. Lett.* **48**, 1559-1562 (1982).
9. Laughlin, R. B., Anomalous quantum Hall effect: An incompressible quantum fluid with fractionally charged excitations. *Phys. Rev. Lett.* **50**, 1395-1398 (1983).
10. Wu, Y.-S., General theory for quantum statistics in two dimensions. *Phys. Rev. Lett.* **52**, 2013-2106 (1984).
11. Tao, R. & Wu, Y. S., Gauge invariance and fractional quantum Hall effect. *Phys. Rev. Lett.* **30**, 1097-1098 (1984).
12. Niu, Q, Thouless, D. J. & Wu, Y. S. , Quantized Hall conductance as a topological invariant. *Phys. Rev. B* **31**, 3372-3377 (1985).
13. Girvin, S. M. & MacDonald, A. H., Off-diagonal long-range order, oblique confinement, and the fractional quantum Hall effect. *Phys. Rev. Lett.* **58**, 1252-1255 (1987).
14. Zhang, S. C. , Hansson, T. H. & Kivelson, S., Effective-field-theory model for the fractional quantum Hall effect. *Phys. Rev. Lett.* **62**, 82-85 (1989).
15. Blok, B. & Wen, X.-G., Effective theories of fractional quantum Hall effect at generic filling fractions. *Phys. Rev. B* **42**, 8133-8144 (1990).
16. Read, N., Excitation structure of the hierarchy scheme in the fractional quantum Hall effect. *Phys. Rev. Lett.* **65**, 1502-1505 (1990).

17. Wen, X.-G. & Zee, A. , A classification and matrix formulation of the abelian FQH states. *Phys. Rev. B* **46**, 2290-2301 (1992).
18. Kitaev, A. Y., Fault-tolerant quantum computation by anyons. *Ann. of Phys. (N. Y.)* **303**, 2-30 (2003).
19. Dennis, E., Kitaev A., Landahl, A. & Preskill, J., Topological quantum memory. *J. Math. Phys.* **43**, 4452-4505 (2002).
20. Freedman, M. H., Kitaev, A., Larsen, M. J. & Wang, Z., Topological quantum computation. *Bull. Amer. Math. Soc.* **40**, 31-39 (2003).
21. Nayak, C., Simon, S. H., Stern, A., Freeman, M. & Das Sarma, S. ankar, Non-Abelian anyons and topological quantum computation. *Rev. Mod. Phys.* **80**, 1083-1159 (2008).
22. Bravyi, S. B., & Kitaev, A.Y., Quantum codes on a lattice with boundary. Preprint at <https://arXiv:quant-ph/9811052> (1998).
23. Rowell E., Stong, R. & Wang, Z., On classification of modular tensor categories, *Comm. Math. Phys.* **292**, 343-389 (2009).
24. Han, Y.-J., Raussendorf, R & Duan, L.-M., Scheme for demonstration of fractional statistics of anyons in an exactly solvable model. *Phys. Rev. Letts.* **98**, 150404 (2007).
25. Zhong, Y. P., Xu, D., Wang, P., Song, C., Guo, Q. J., Liu, W. X., Xu, K., Xia, B. X., Lu, C.-Y., Han, S. Y., Pan, J.-W. & Wang, H., Emulating anyonic fractional statistical behavior in a superconducting quantum circuit. *Phys. Rev. Letts.* **117**, 110501 (2016).

26. Luo, Z. H., Li, J., Li, Z., Hung, L.-Y., Wan Y., Peng, X., & Du, J. F., Experimentally probing topological order and its breakdown through modular matrices. *Nat. Phys.* **14**, 160-166 (2018).
27. Li, Keren Li, Wan, Y. D., Huang, L.-Y. Hung, Lan, T., Long, G. L., Lu, D. W., Zeng, B. & Laflamme, R., Experimental identification of non-Abelian topological orders on a quantum simulator. *Phys. Rev. Letts.* **118**, 080502 (2017).
28. Jiang, H.-C., Wang, Z. H., & Balents, L., Identifying topological order by entanglement entropy. *Nat. Phys.* **8**, 902-905 (2012).
29. Wen, X. G. , Colloquium: Zoo of quantum-topological phases of matter. *Rev. Mod. Phys.* **89**, 041004 (2017).
30. Mignard, M., & Schauenburg, P., Modular categories are not determined by their modular data. Preprint at [https://arXiv: 1708.02796](https://arXiv:1708.02796) (2017).
31. Kitaev, A. & Kong, L., Models for gapped boundaries and domain walls. *Comm. Math. Phys.* **313**, 351-373 (2012).
32. Kong, L., Wen, X.-G. & Zheng, H., Boundary-bulk relation in topological orders. *Nucl. Phys. B* **922**, 62-76 (2017).
33. Kong, L., Anyon condensation and tensor categories. *Nucl. Phys. B* **886**, 436-482 (2014).
34. Kong, L. & Zheng, H., A mathematical theory of gapless edges of 2d topological orders. Part I. *J. High Energ. Phys.* **2020**, 150 (2020).

35. Kong, L. & Zheng, H., A mathematical theory of gapless edges of 2d topological orders. Part II. Preprint at [https://arXiv: 1912.01760](https://arXiv:1912.01760) (2019).
36. Etingof, P., Gelaki, S., Nikshych, D. & Ostrik, V., *Tensor Categories* (American Mathematical Society, Providence, RI, 2015).
37. Aharonov, Y. & Bohm, D., Significance of electromagnetic potentials in the quantum theory. *Phys. Rev.* **115**, 485-491 (1959).
38. Wen, X. G., Quantum orders in an exact soluble model. *Phys. Rev. Lett.* **90**, 016803 (2003).
39. Fowler, A. G., Mariantoni, M., Martinis, J. M. & Cleland, A. N., Surface codes: Towards practical large-scale quantum computation. *Phys. Rev. A.* **86**, 032324 (2012).
40. Cong, I. and Cheng, M. & Wang, Z., Universal quantum computation with gapped boundaries. *Phys. Rev. Lett.* **119**, 270504 (2017).
41. Cong, I. and Cheng, M. & Wang, Z., Topological quantum computation with gapped boundaries. Preprint at [https://arXiv: 1609.02037](https://arXiv:1609.02037) (2016).

Acknowledgements We would like to thank Y.-S. Wu, D. Lu, J. Ye, W. Chen, Z. Tao and Y. Chen for their helpful discussion. J. W. would also like to thank D. Lu for providing the facility of the NMR quantum computing experiments. J. W. was supported by National Natural Science Foundation of China (Grant No. 11674152 and No. U1801661), Guangdong Innovative and Entrepreneurial Research Team Program (No. 2016ZT06D348), Natural Science Foundation of Guangdong Province (Grant No. 2017B030308003) and Science, Technology and Innovation Commission of Shenzhen Municipality (Grant No. JCYJ20170412152620376).

and No. KYTDPT20181011104202253). J. W., L. K. and H. Z. are supported by the Science, Technology and Innovation Commission of Shenzhen Municipality (Grant No. ZDSYS20170303165926217) and Guangdong Provincial Key Laboratory (Grant No.2019B121203002). L. K. is supported by NSFC under Grant No. 11971219. H. Z. is supported by NSFC under Grant No. 11871078.

Author contributions L. K. and J. W. initiated the project. L. K. proposed the main idea and J. W. worked out the detailed theory and experimental implement scheme on the toric code model. Y.-J. H, worked on part of the theory and did the proposed experiment on the quantum cloud. Z. Z. did the NMR experiments on the NMR quantum computing system. J. W monitored their work. H. Z. worked out the subtle part of the theory. Y.-J. H., L. K. and J. W. wrote the draft and J. W. conceived all the inputs from all authors. D. Y. supervised the whole project. All authors contributed to discussing the results.

Competing Interests The authors declare that they have no competing financial interests.

Correspondence Correspondence and requests for materials should be addressed to Liang Kong (email: kongl@sustech.edu.cn) and Jiansheng Wu (email: wujs@sustech.edu.cn).

Table 1: The bulk anyons defined by boundary excitations and the bulk anyon braidings defined by the half braidings of boundary excitations

a) The bulk anyons defined by the boundary excitations and half braidings
$1 = (1, 1 \otimes 1 = 1 \xrightarrow{1} 1 = 1 \otimes 1, 1 \otimes e = e \xrightarrow{1} e = e \otimes 1)$
$m = (1, 1 \otimes 1 = 1 \xrightarrow{1} 1 = 1 \otimes 1, 1 \otimes e = e \xrightarrow{-1} e = 1 \otimes e)$
$e = (e, e \otimes 1 = e \xrightarrow{1} e = 1 \otimes e, e \otimes e = 1 \xrightarrow{1} 1 = e \otimes e)$
$\varepsilon = (e, e \otimes 1 = e \xrightarrow{1} e = 1 \otimes e, e \otimes e = 1 \xrightarrow{-1} 1 = e \otimes e)$
b) The bulk anyon braidings defined by the half braidings of boundary excitations
$1 \otimes x = x \xrightarrow{c_{1,x}=1} x = x \otimes 1, \text{ for } x = 1, e, m, \varepsilon$
$x \otimes x = 1 \xrightarrow{c_{x,x}=1} 1 = x \otimes x, \text{ for } x = 1, e, m$
$\varepsilon \otimes \varepsilon = 1 \xrightarrow{c_{\varepsilon,\varepsilon}=-1} 1 = \varepsilon \otimes \varepsilon$
$e \otimes m = \varepsilon \xrightarrow{c_{e,m}=1} \varepsilon = m \otimes e$
$m \otimes e = \varepsilon \xrightarrow{c_{m,e}=-1} \varepsilon = e \otimes m$
$e \otimes \varepsilon = m \xrightarrow{c_{e,\varepsilon}=1} m = \varepsilon \otimes e$
$\varepsilon \otimes e = m \xrightarrow{c_{\varepsilon,e}=-1} m = \varepsilon \otimes e$
$m \otimes \varepsilon = e \xrightarrow{c_{m,\varepsilon}=-1} e = \varepsilon \otimes m$
$\varepsilon \otimes m = e \xrightarrow{c_{\varepsilon,m}=1} e = m \otimes \varepsilon$

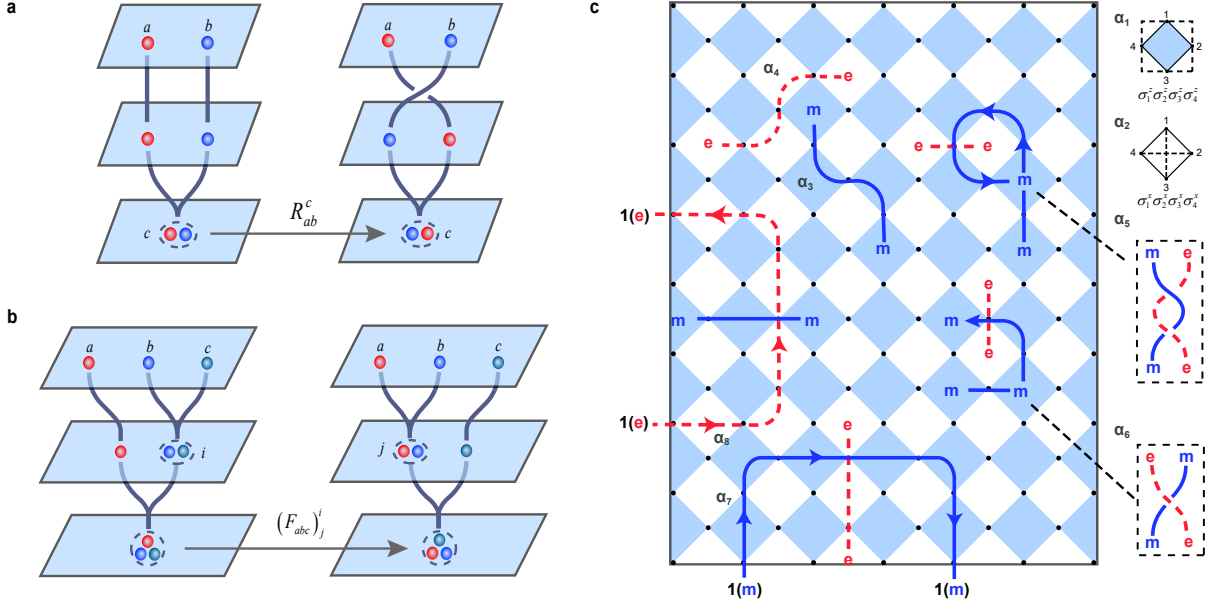


Figure 1: **Graphical representation of the R -matrices, the F -matrices and a toric code lattice with gapped boundaries.** **a**, Braiding of two anyons and the definition of the R -matrices; **b**, Fusion of three anyons in different orders and the definition of the F -matrices; **c**, Toric code lattice with boundaries. α_1 and α_2 are the two elementary plaquettes, the blue plaquette and the white plaquette. α_3 and α_4 are the string operators for generating an m anyon pair and an e anyon pair, respectively. α_5 and α_6 visualize the double braiding and braiding operations. Double braiding corresponds to moving an m (e) anyon around an e (m) anyon along a full circle, which generates an overall phase of -1 . Braiding corresponds to the exchange of an m anyon and an e anyon: If they are in the bulk, the state after braiding is different from the initial state. α_7 and α_8 are half braidings at the white (smooth) and blue (rough) boundaries. At a white boundary, an m anyon is equivalent to vacuum state 1. Dragging an m anyon from the vacuum state, moving it around a boundary excitation e along a semicircle and pushing it back out results in a phase difference of -1 . The case is similar for a blue boundary.

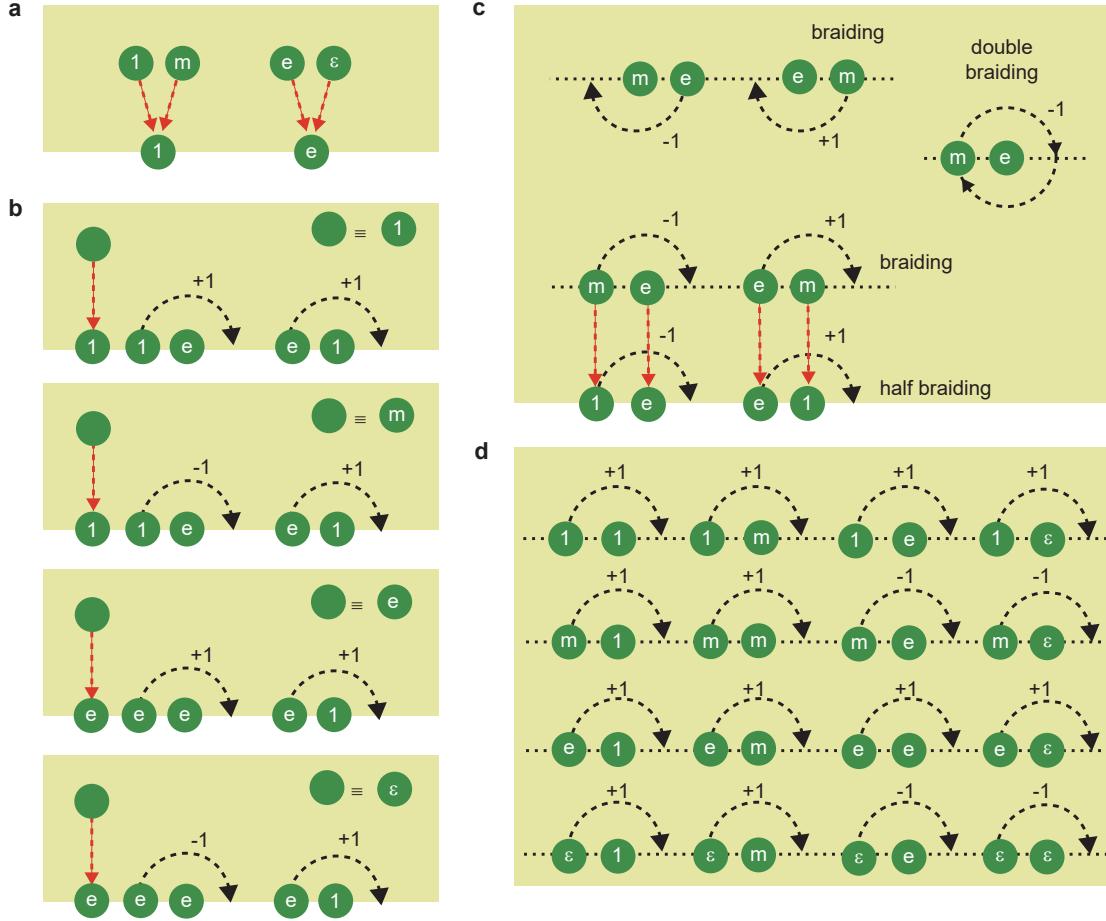


Figure 2: **Illustrations of half braidings, braidings and double braidings.** **a**, There are 4 kinds of bulk anyons in the bulk and 2 kinds of boundary excitations. m and 1 (e and ε) belong to the same topological sector when they are moved to a white boundary. **b**, Definitions of the 4 kinds of bulk anyons using the half braidings on the boundary. m and 1 are different when they are equipped with different half braidings, as are ε and e . **c**, Braidings in the bulk defined in terms of the half braidings on the boundary. The black dotted line represents a virtual boundary in the bulk. By moving bulk anyons to the boundary, and using the half braidings of the boundary excitations, the braidings of the bulk anyons can be defined. There are two equivalent sets of braidings (the set above the virtual boundary and the set below it) and the double braidings can be obtained from these braidings as well. **d**, A complete list of braidings for the 4 kinds of bulk anyons.

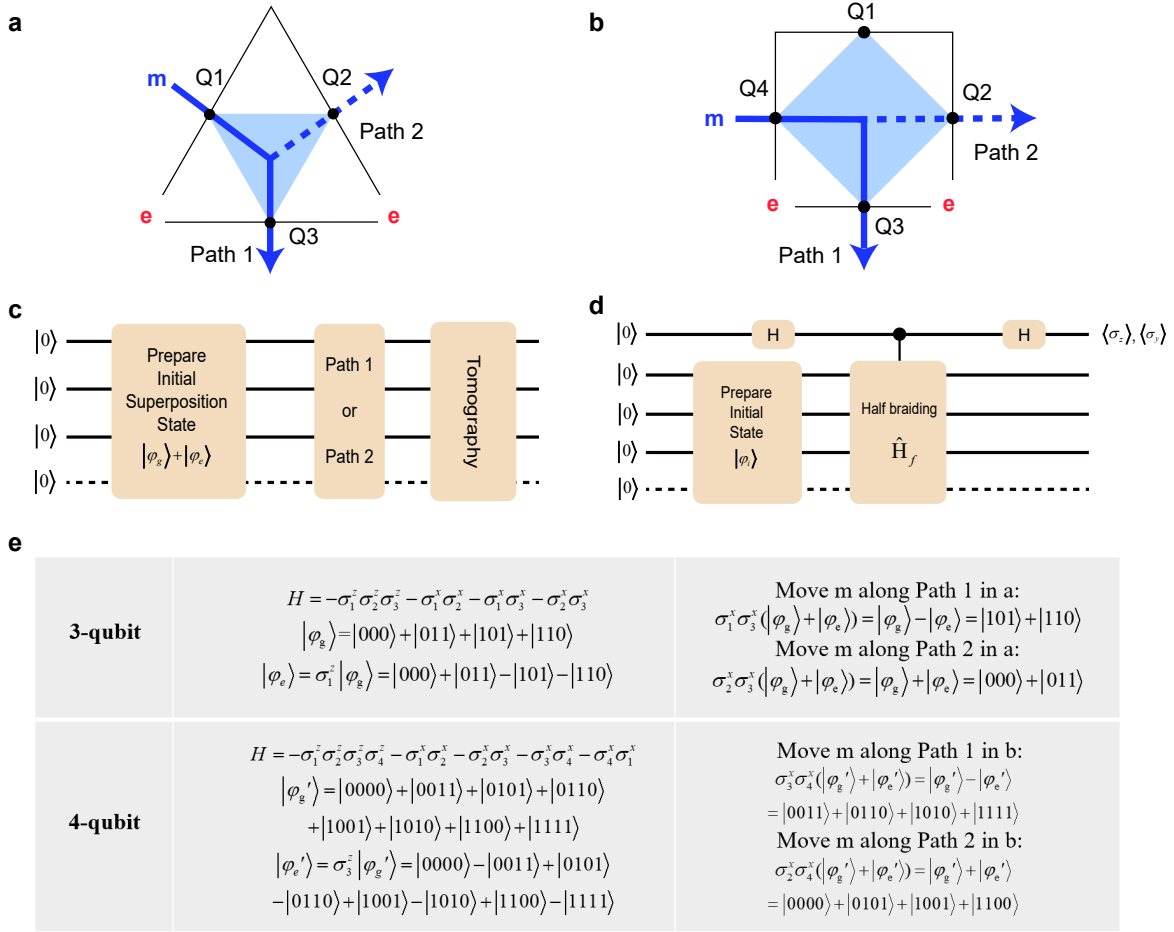


Figure 3: Illustrations of the experimental setups and corresponding quantum states. **a**, A 3-qubit toric code model and the half braidings of m along Path 1 and Path 2. **b**, A 4-qubit toric code model and the half braidings of m along Path 1 and Path 2. **c**, Quantum circuit for measuring m - e half braidings on a white (smooth) boundary. First, the initial state $|\varphi_g\rangle + |\varphi_e\rangle$ is prepared in the first step, where $|\varphi_g\rangle$ is the ground state and $|\varphi_e\rangle$ represents the excited state with two boundary e excitations. Moving the m anyon through the Path 1 and Path 2 by applying a series of σ_x operators to the qubits involved in these paths leads to the states $|\varphi_g\rangle - |\varphi_e\rangle$ and $|\varphi_g\rangle + |\varphi_e\rangle$, respectively. These two states can be differentiated via quantum state tomography. **d**, Quantum circuit for general phase measurement. The state before half braiding is prepared as the initial state $|\varphi_i\rangle$, and a half braiding is performed as a controlled operation. For the general Abelian anyon model, a half braiding operation generates a phase factor, which can be obtained from the two expectation values $\langle\sigma_z\rangle$ and $\langle\sigma_y\rangle$ on the ancilla qubit. **e**, The Hamiltonians and initial and final states of the half braiding processes for the 3- and 4-qubits systems.

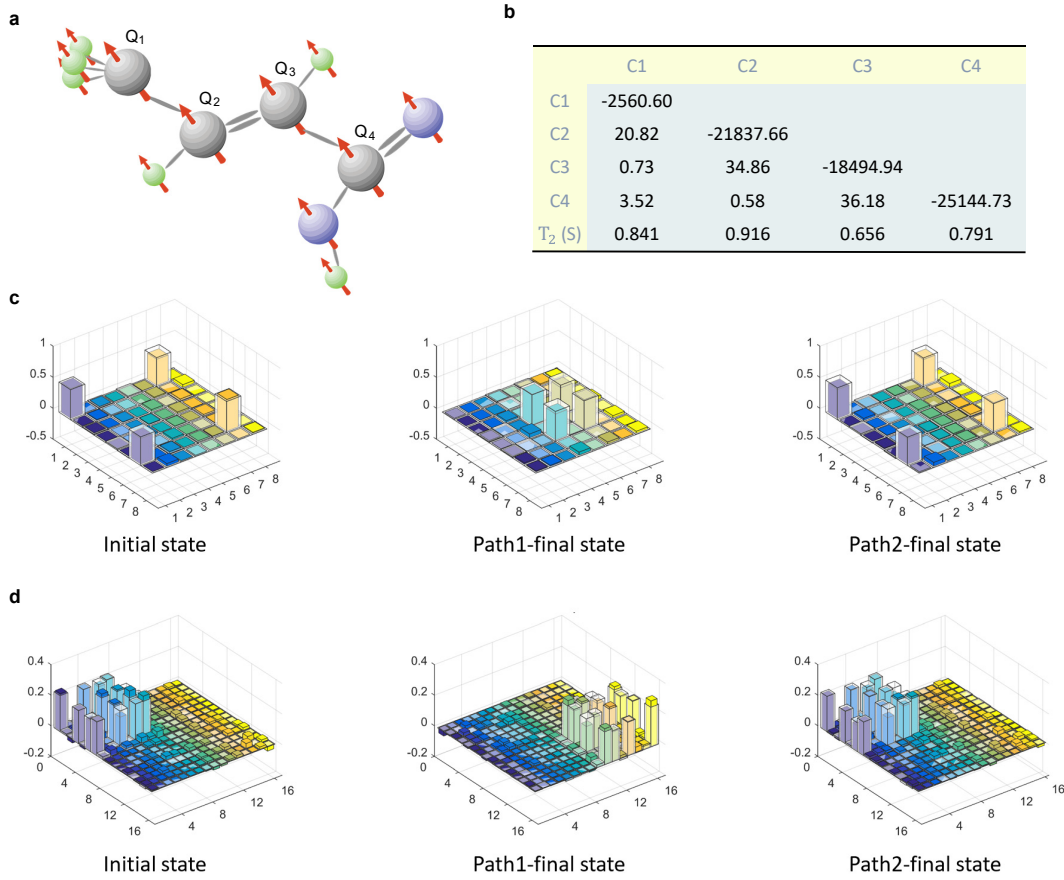


Figure 4: The experimental platforms and the results of quantum state tomography. **a**, Our 3, 4-qubit quantum simulator is a sample of ^{13}C -labeled trans-crotonic acid molecules. We make 4 ^{13}C atoms from the sample as 4 qubits. **b**, The table on the right lists the parameters of the chemical shifts (diagonal, Hz), J-coupling strengths (off-diagonal, Hz), and relaxation time scales T_2 (seconds). **c**, State tomography results for the initial and final states obtained when moving m along different paths in the 3-qubit toric code model. The transparent columns represent the theoretical values, and the colored columns represent the experimental results. Regarding the scale of the X axis in each three-dimensional bar graph, 1 represents the state $|0000\rangle$, 2 represents the state $|0001\rangle$ and so on. Compared with the theoretical results, the two final states in the 3-qubit experiments using Path 1 and Path 2 are obtained with fidelities of 96.37% and 96.67%, respectively. **d**, State tomography results for the final states obtained by moving m along different paths in the 4-qubit toric code model. Compared with the theoretical results, the two final states in the 4-qubit experiments using Path 1 and Path 2 are obtained with fidelities of 95.23% and 95.21%, respectively.

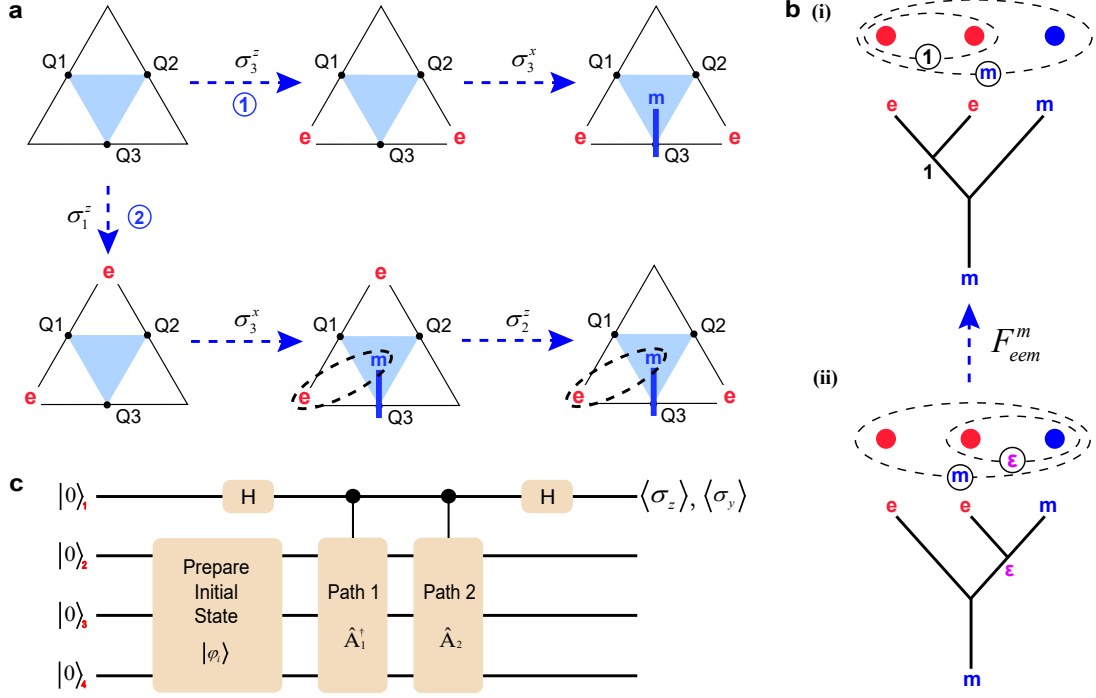


Figure 5: **Two fusion diagrams and the measurement of the F -matrix.** **a**, Two different fusion processes on a 3-qubit plaquette represented by two paths. **b**, The circle notation and fusion tree diagrams for Path 1 and Path 2 in (a). **c**, The scattering circuit used to measure the overlap of the final states of the two paths, where $\hat{A}_1 = \sigma_3^x \sigma_3^z$, and $\hat{A}_2 = \sigma_2^z \sigma_3^x \sigma_1^z$. The value of the overlap yields F_{eem}^m .